JACS
JOURNAL OF THE AMERICAN CHEMICAL SOCIETY
pubs.acs.org/JACS
Article

Enhanced CO_2 Reactive Capture and Conversion Using Aminothiolate Ligand−Metal Interface

Mingyu Wan,[⊥] Zhengyang Yang,[⊥] Heba Morgan, Jinquan Shi, Fan Shi, Mengxia Liu, Hsi-Wu Wong, Zhiyong Gu,* and Fanglin Che*

Cite This: J. Am. Chem. Soc. 2023, 145, 26038−26051
Read Online
ACCESS | Metrics & More | Article Recommendations | Supporting Information

ABSTRACT: Metallic catalyst modification by organic ligands is an emerging catalyst design in enhancing the activity and selectivity of electrocatalytic carbon dioxide (CO_2) reactive capture and reduction to value-added fuels. However, a lack of fundamental science on how these ligand−metal interfaces interact with CO_2 and key intermediates under working conditions has resulted in a trial-and-error approach for experimental designs. With the aid of density functional theory calculations, we provided a comprehensive mechanism study of CO_2 reduction to multicarbon products over aminothiolate-coated copper (Cu) catalysts. Our results indicate that the CO_2 reduction performance was closely related to the alkyl chain length, ligand coverage, ligand configuration, and Cu facet. The aminothiolate ligand−Cu interface significantly promoted initial CO_2 activation and lowered the activation barrier of carbon−carbon coupling through the organic (nitrogen (N)) and inorganic (Cu) interfacial active sites. Experimentally, the selectivity and partial current density of the multicarbon products over aminothiolate-coated Cu increased by 1.5-fold and 2-fold, respectively, as compared to the pristine Cu at −1.16 V_{RHE}, consistent with our theoretical findings. This work highlights the promising strategy of designing the ligand−metal interface for CO_2 reactive capture and conversion to multicarbon products.

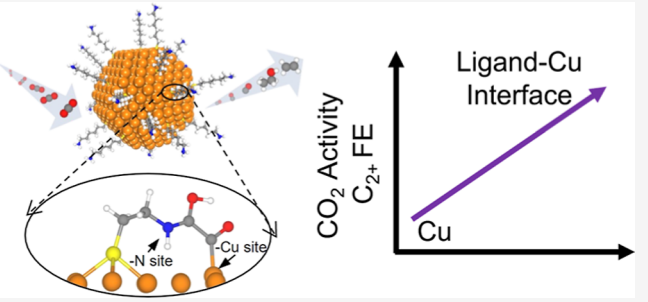

INTRODUCTION

In recent years, excessive utilization of fossil fuels has caused increasing carbon dioxide (CO_2) concentration in the atmosphere and thus a severe global climate threat.[1] CO_2 reactive capture[2−5] and conversion,[6] for example, electrochemical CO_2 capture and CO_2 reduction reaction (CO_2RR) into value-added hydrocarbons and alcohols, become a promising strategy to close the carbon loop and form a net-zero-carbon process.[7] CO_2 can be converted through diverse approaches, such as biochemical,[8] thermochemical,[9] electrochemical,[10] photochemical reactions,[11,12] and microwave.[13,14] Among these approaches, electrocatalytic CO_2 capture and reduction, powered by renewable electricity, is attractive because it has several advantages, including mild operating conditions, controllable reaction rates by tuning parameters like applied potentials, pH, and electrolyte anion/cation and economic feasibility.[15] In this regard, copper (Cu)-based materials have received the most attention because Cu is, so far, the only cost-effective transition-metal catalyst that could achieve multicarbon products via CO_2RR, such as ethylene and ethanol.[16] However, the following challenges[17] remain for CO_2RR using Cu-based catalysts: (1) CO_2RR to a multicarbon product requires a high applied potential (∼−1.0 V vs reversible hydrogen electrode (RHE)), which could lead to Cu surface reconstruction, and thus catalyst deactivation; (2) the initial capture and activation of CO_2 demands high energy; (3) Cu can catalyze CO_2 to a variety of hydrocarbons, but a way to control the selectivity of CO_2RR to a single desired multicarbon product is still lacking.

Ligand−metal catalytic interfaces have been widely used in thermal catalysis.[18] With well-defined compositions of ligands, that is, head and tail functional groups, the modulated catalysts have shown enhancement in the activity and selectivity to a desired product, mainly through steric and electronic effects.[19] Steric effects refer to a high density of ligands that could induce a confined space to tune the configurations of the adsorbates or selectively expose specific surface sites, so that the reaction could proceed in the desired direction.[20−22] For example, Medlin and co-workers[21] modified palladium (Pd) catalysts with self-assembled monolayers (SAMs) to improve the selectivity of furfural hydrogenation to desired furfuryl alcohol and methylfuran rather than furan and tetrahydrofuran. This improvement in selectivity is due to the high density of

Received: June 29, 2023
Revised: November 1, 2023
Accepted: November 3, 2023
Published: November 16, 2023

https://doi.org/10.1021/jacs.3c06888
J. Am. Chem. Soc. 2023, 145, 26038−26051

Scheme 1. Proposed Mechanism for CO_2RR to Multicarbon Products over C_2 Ligand-Coated Cu Interface and Its Competitive HER[a]

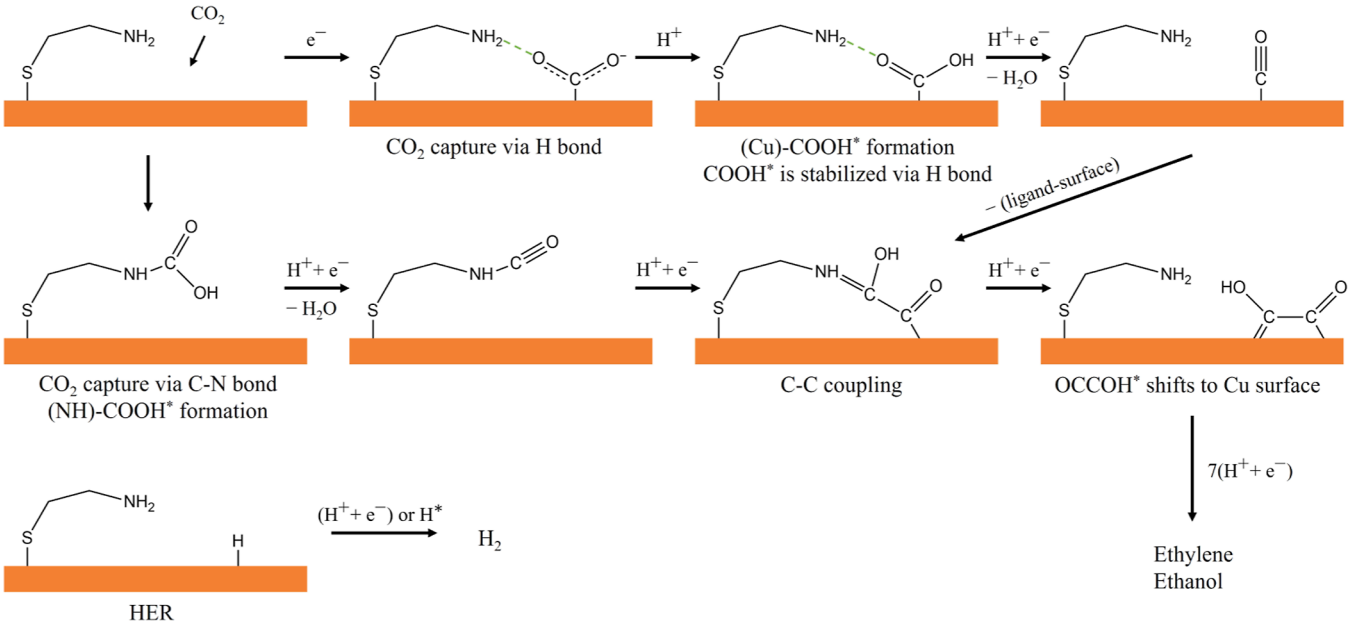

[a]This mechanism applies to C_6 and C_{11} ligands. COOH* formation and C−C coupling are the possible rate-determining steps. Green dash lines represent the H bond.

SAM ligands that provide confined space, forcing the adsorption of furfural over Pd via an upright configuration at the edge or defect sites and selectively blocking the terrace sites of furfural decarboxylation to undesired furan and tetrahydrofuran. As for the electronic effect, the surface ligands could control the selectivity by modulating the near-surface electrostatics via Lewis acid−base interactions.[23,24] Chen et al.[23] reported that during the partial hydrogenation of nitrobenzene to *N*-hydroxylanilines, the electron donation from ethylenediamine ligands to platinum (Pt) nanowires makes the catalytic surface become electron-rich, favoring the adsorption of electron-deficient *N*-hydroxylanilines and preventing its full hydrogenation into anilines.

The application of ligand−metal interface in electrocatalysis, for example, CO_2RR,[6,25,26] has attracted more attention. A critical advantage of sulfur (S)-based surface ligands (e.g., thiolates) is that with the strong sulfur−metal bond, the surface energies of the catalysts significantly decrease, suppressing the metallic surface reconstruction and thus enhancing the stability of the catalysts at a high applied potential.[27,28] Besides, the microenvironment (e.g., local pH, cation/anion concentration, and surface reactants) at the electrode/electrolyte interfaces could be controlled by surface ligands.[29] For instance, Banerjee et al.[30,31] reported that the cationic surfactant, cetyltrimethylammonium bromide, can bind to a Cu electrode via electrostatic attraction and displace hydronium and hydrated alkali cations, which diminishes the local proton sources for hydrogen evolution reaction (HER) and enhances the selectivity of CO_2RR to CO and HCOOH. Another advantage of surface ligands in electrocatalysis is that well-designed tail groups of the surface ligands could directly interact with the reactant CO_2. Due to the amine group's capability to capture CO_2,[32−35] it is usually designed as the tail group of the organic ligands for CO_2 capture and activation.[36−42] Sandru et al.[43] designed a high-solubility and fast-diffusion membrane by growing an ultrathin amine-containing surface layer on a supported high-permeability polymer thin film for CO_2 capture. Taken together, modified Cu catalysts using organic ligands with a sulfur headgroup and an amine tail group (i.e., aminothiolates) could potentially enhance CO_2 reactive capture and conversion. However, the lack of fundamental science elaborating how the physical factors (e.g., ligand surface coverage, alkyl chain length, ligand configuration, or surface facet) of the ligand−metal interface interact with CO_2RR intermediates under working conditions limits the electrocatalyst design using surface ligands.

In this work, we first performed density functional theory (DFT) to systematically study how aminothiolate ligand-coated Cu catalyst promotes CO_2 conversion to multicarbon products. The ligands' configuration, coverage, alkyl chain length effects, and surface facets were considered. Two configurations, including "flat-lying" and "upright", were studied. We varied the ligand surface coverages from 1/16 monolayer (ML) to 8/16 ML. As for the alkyl chain lengths, we investigated cysteamine (C_2), 6-amino-1-hexanethiol (C_6), and 11-amino-1-undecanethiol (C_{11}). Inspired by our previous work,[44] we introduced dual-active sites (organic nitrogen site (N) and inorganic Cu site) for CO_2 activation and its following electron transfer reduction step. The activity and selectivity were evaluated by the potential rate-determining steps (RDS) during CO_2 to multicarbon products, that is, COOH* formation and carbon−carbon (C−C) coupling (Scheme 1).[45−48] We also discuss HER performance. The simulations were performed on the most active Cu(100) and the most stable Cu(111) facet. In addition, this is the first time that we have shown the corresponding proof-of-concept experiments to validate our theoretical predictions. We coated aminothiolates on a Cu foil and confirmed the existence of the thiolate-type Cu−S bond after the coating and after the CO_2RR. We further operated CO_2RR in an H-cell setup to verify the effects of the ligand−metal interface on promoting the activity and selectivity of CO_2RR to multicarbon products

https://doi.org/10.1021/jacs.3c06888
J. Am. Chem. Soc. 2023, 145, 26038−26051

(ethylene, ethanol, acetic acid, acetaldehyde, and propionaldehyde) compared to the pristine Cu.

RESULTS AND DISCUSSION

Ligand Stability. Ligand alkyl chain lengths, surface coverages, and Cu facets can significantly influence the most favorable ligand configuration (i.e., flat-lying and upright) adsorbed over the surface and, consequently, alter the surface stability.[49−51] We first examined the effect of ligand alkyl chain lengths of aminothiolates ($NH_2-C_nH_{2n}-S$, n = 2, 6, 11, represented by C_n in the following text) on their surface adsorption over Cu(100) (C_n/Cu(100)) with both flat-lying and upright configurations along with their differential charge analysis (Figure 1). The result shows that the flat-lying configuration has more electron transfer with the surface because both the head and tail groups can interact with Cu, while the ligand with the upright configuration only interacts with the surface through the headgroup. The differential charge analysis is consistent with our adsorption energy calculations (Figures S1 and S2). The results show that C_2 prefers a flat-lying configuration when the surface ligand coverage is ≤ 4/16 ML. As the coverage increases to 8/16 ML, C_2 can only exist as an upright configuration. The reason is that although the flat-lying configuration has a stronger adsorption energy at a low coverage, it occupies more surface sites, resulting in its inability to exist at a high surface coverage. Similar results can be obtained from the scenarios for C_6 and C_{11}. The difference is that at a surface coverage of ≥4/16 ML, C_6 and C_{11} can only exist in upright configurations. It is worth noting that C_{11} at a coverage of 2/16 ML is a configuration state in between flat-lying and upright, that is, at an angle less than 90 degrees to the surface, which agrees well with another theoretical study regarding the configuration of thiolates with various alkyl chain lengths.[50] We note that neither the flat-lying nor the upright configuration is easily protonated during electrocatalytic CO_2RR. For the flat-lying configuration, the amine group bonds to the Cu surface, preventing protonation. This is confirmed by a previous report,[36] which investigated the aminothiolate-coated Ag surface. For the upright configuration, our Pourbaix diagram[44] indicates that the protonation of the amine group is thermodynamically unfavorable under a common CO_2RR environment. Overall, the adsorption energies of all three ligands become weaker with increasing surface coverages due to the lateral interactions.[50] Similar conclusions could be found for aminothiolate adsorption on Cu(111) (Figures S3 and S4). The only difference is that C_2/Cu(111) is more favorable with the upright configuration at 4/16 ML because Cu(111) is more compact than Cu(100).

During the CO_2RR electrocatalysis, a negative bias with reference to RHE is applied to the electrode, which might lead to thiolate reduction to thiol and subsequent desorption (Figure 2a). Therefore, we applied the computational standard hydrogen electrode (CHE) model[52] (see Supporting Information) to establish the Pourbaix diagram (Figure S5) and examined the stability of aminothiolate ligands with various

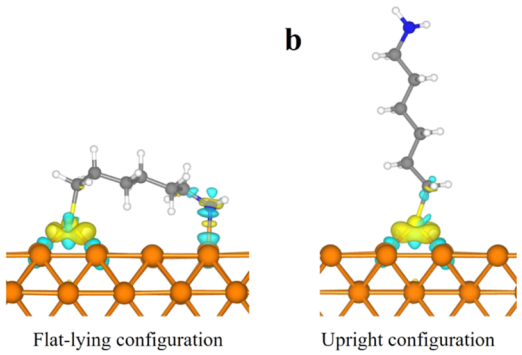

Figure 1. Differential charge analysis for C_6 ligand adsorption over Cu(100) with both (a) flat-lying and (b) upright configurations. The isosurface is 0.004 e/bohr.[3] Yellow and blue areas represent the gain and loss of electrons, respectively. Color code: Cu (orange), S (yellow), C (gray), N (blue), and H (white).

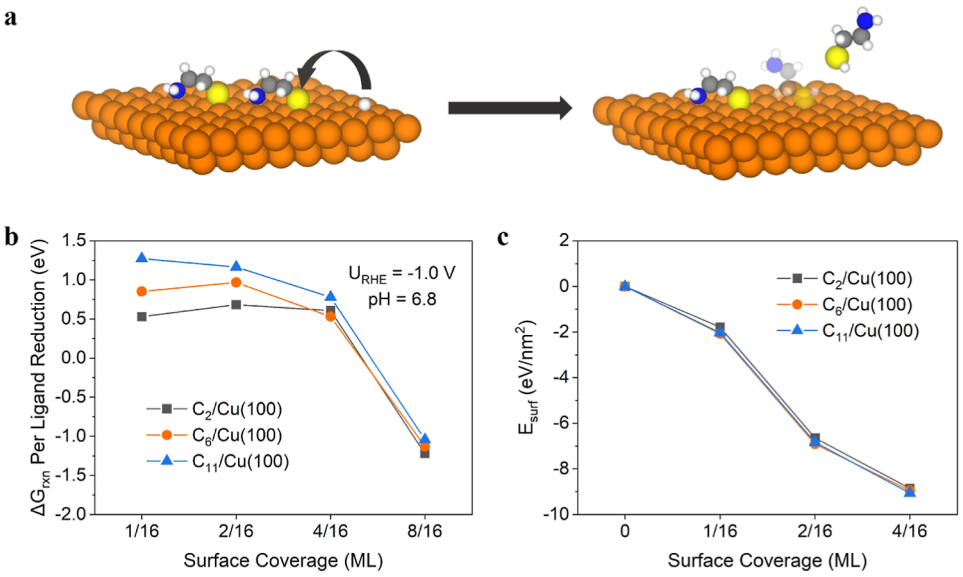

Figure 2. Stability of the ligand−Cu(100) interface. (a) Scheme of possible thiolate reduction to thiols and desorption from the surface. Color code refers to Figure 1; (b) Gibbs reaction free energy of the ligands with different chain lengths under the CO_2RR to multicarbon product operation conditions; and (c) surface formation energy of the ligands with three alkyl chain lengths at various surface coverages. The reference surface formation energy was set to be the bare Cu surface, i.e., ligand surface coverage of 0 ML.

https://doi.org/10.1021/jacs.3c06888
J. Am. Chem. Soc. 2023, 145, 26038−26051

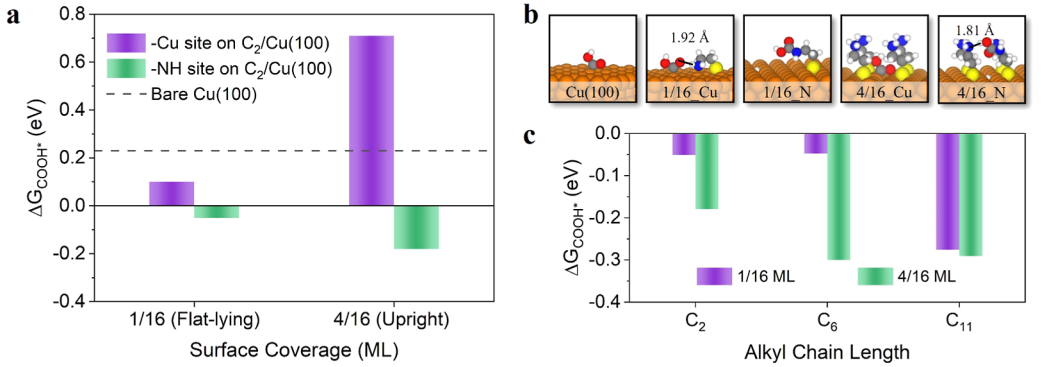

Figure 3. CO_2 activation (* + CO_2 + H^+ + e^- → COOH*) on Cu(100) at pH = 6.8 and U = −1.0 V_{RHE}. (a) COOH* formation energy in the presence and absence of C_2 aminothiolate ligands involving the effect of coverage (i.e., 1/16 and 4/16 ML), configurations, and dual-active sites (i.e., Cu and N sites); (b) geometries corresponding to each point in a H bond and its bond length are labeled. Color code: Cu (orange), S (yellow), C (gray), N (blue), O (red), and H (white); and (c) COOH* formation energy at the N site for C_2, C_6, and C_{11} ligands at the coverages of 1/16 and 4/16 ML.

alkyl chain lengths and surface coverages over Cu(100) and Cu(111) under various electrocatalytic working conditions. The Gibbs free reaction energy (ΔG_{rxn}) of per ligand reduction is calculated through the following elementary step

$$n\text{thiolates/Cu} + H^+ + e^- \rightarrow \text{thiol} + (n-1)\text{thiolates/Cu} \quad (1)$$

Under the operation condition of CO_2RR to multicarbon products (pH = 6.8, U = −1.0 V_{RHE}),[46,47,53] when the coverage is below 8/16 ML, the above reaction on Cu(100) is endothermic, meaning these thiolates are potentially stable to adsorb on the surface (Figure 2b). However, as the coverage increases to 8/16 ML, this reductive step becomes exothermic, representing that thiolate reduction could occur spontaneously. Thus, the maximum surface coverage of aminothiolates over Cu(100) is 4/16 ML. In addition, the ligand with a longer alkyl chain length (i.e., C_{11}) is more stable at each surface coverage (Figure 2b). This might be because the thiolates with longer alkyl chains are stabilized by the intermolecular interactions.[54,55] Our simulation trend of the alkyl chain effect is consistent with a recent experimental study,[56] in which the peaks from the reductive desorption linear sweep voltammograms shift to more negative potentials with the increasing alkyl chain length of alkanethiolate on Au, suggesting that the thiol-based ligand with a longer alkyl chain results in a higher ligand stability over the metal surface.

To estimate the stability of the catalyst in the presence of surface ligands, we calculated the Cu surface formation energy (E_{surf}) by eq S2. E_{surf} decreases monotonically with increasing ligand coverages (Figure 2c), meaning the Cu surface can be stabilized by the deposition of surface ligands, consistent with the literature.[27,28] Cu open/defect sites are prone to undergo surface reconstruction during electrocatalysis.[16] To investigate the ligand effects on these open/defect sites, Cu(100) with adatom-induced defect surfaces and a Cu(211) kink surface were taken into the stability test. The results shown in Figure S6 indicate that the presence of the thiolate ligand stabilizes both high-index and reconstructed surfaces. However, unlike the significant reconstructed Au atoms caused by the thiolate ligand in the previous literature,[57,58] the obvious reconstructed Cu atoms are not observed in the structures. This suggests that the Cu sites could still remain active. In addition, the aminothiolate ligand induces an additional active N site, which is not affected by the surface reconstruction. As for the ligand stability over Cu(111), the results are similar to those over Cu(100) (Figure S7). Over Cu(111), C_2 thiolates at the coverage of 4/16 ML become unfavorable under a high applied potential because its reduction energy is negative. All three aminothiolates at a high coverage (8/16 ML) become much less stable with a more exothermic ΔG_{rxn} due to their compact surface space.

Previous experimental studies indicated that when thiols deposit on metal surfaces, such as Pt,[59] Au,[55] and Cu,[60] there is a possibility that the S−C bond could break due to the strong bond strength between S and metal sites, consequently leading to S poisoning the surface. To examine the possibility of S poisoning over the Cu surface, we calculated the activation barriers of S−C bond cleavage for C_2 ligand adsorption at a coverage of 1/16 ML on Cu(100) (Figure S8) as a case study. Our results show that although S−C bond cleavage is an exothermic process with a reaction energy of −0.49 eV, a very high activation barrier of 1.05 eV must be overcome to break the S−C bond. This reaction is potential-independent and will be less likely to occur at the room temperature, that is, CO_2RR condition. As for 4/16 ML, however, there is no sufficient space over the Cu surface for the remaining part (i.e., $C_2H_4NH_2$) to adsorb after the S−C bond cleavage. Thus, after S−C bond cleavage, the remaining part of thiolate might diffuse and be reduced in the solution. To determine the dissociation barrier of S−C bond cleavage, we then artificially enlarged the distance between S and C atoms of the thiolate and performed single-point calculations. Our results (Figure S9) indicate that as the distance increases, the energy required to break the bond increases until it reaches a plateau. From the calculation of thiolate S−C bond cleavage at a low surface coverage of 1/16 ML, we measured the bond distance between S and C atoms at the transition state of ∼2.57 Å. Taking this into Figure S9, we can see that breaking the S−C bond of the 4/16 ML ligand needs ∼2 eV, which is higher than that at a lower coverage (1.05 eV). This is consistent with our expectation that as the surface coverage of thiolates over the Cu surfaces increases, the Cu−S bond will be weakened due to the surface lateral interactions, strengthening the S−C bond.

We further calculated the reaction energy of the S−C bond cleavage for C_6 and C_{11} over Cu(100) (Figure S10). The results indicate that, with the increasing alkyl chain lengths of surface ligands, the reaction energy becomes less exothermic or even endothermic, meaning that the longer aminothiolate might be less likely to break the S−C bond when these

https://doi.org/10.1021/jacs.3c06888
J. Am. Chem. Soc. 2023, 145, 26038−26051

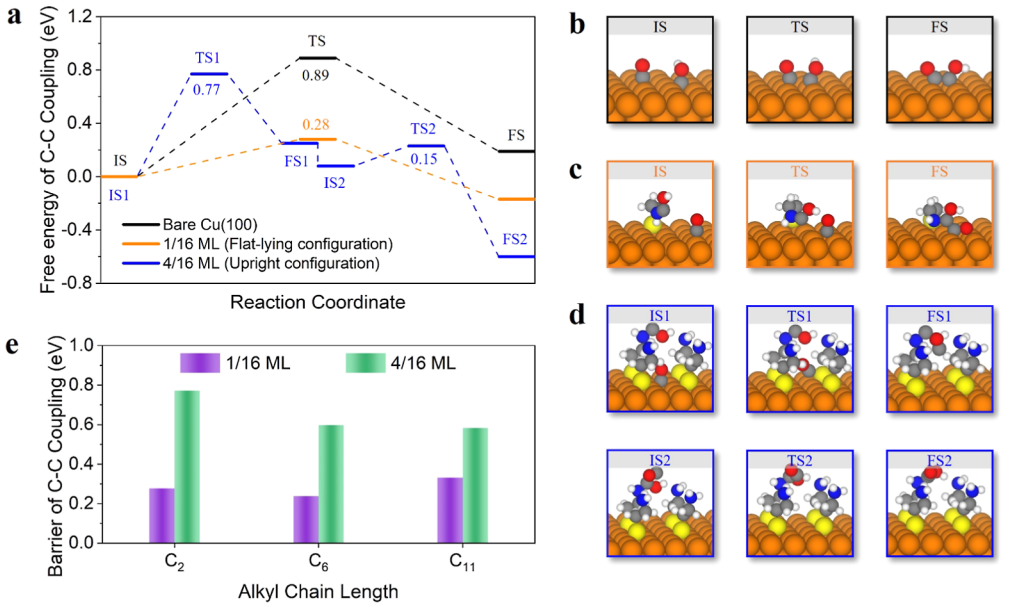

Figure 4. C−C coupling (CO* + COH* → OCCOH* + *) reaction free energies and activation barriers on Cu(100). (a) Free-energy diagram of C−C coupling with and without C_2 ligands. The activation barriers for all the examined cases are indicated in the plot. The corresponding geometries of IS, TS, and FS are shown in (b−d). Color code refers to Figure 3. (e) Activation barrier of C−C coupling over the ligand−metal interface, including C_2, C_6, and C_{11} ligands at 1/16 and 4/16 ML.

reactions obey the Brønsted−Evans−Polanyi relationship where activation barriers increase with the increasing reaction energies.[61−63] Taken together, the aminothiolate ligands are proven to be stable over the Cu surface at a maximum coverage of 1/4 ML for most alkyl chain lengths (except for the C_2 ligand at 1/4 ML over Cu(111)) and suppress the surface reconstruction during electrocatalysis. A more negative applied potential results in a decreased surface coverage of ligands. The ligand−metal stability depends on various factors, including the alkyl chain length, ligand configuration, surface coverage, and Cu facet.

CO_2 Activation. We then examined the role of a stable ligand−metal interface in enhancing the CO_2RR performance. CO_2RR activity was estimated via COOH* formation (* + CO_2 + H^+ + e^- → COOH*) because this is the first electron transfer step to activate CO_2 and the possible RDS for generating the key intermediate CO* (the precursor of the multicarbon products) during CO_2RR.[45] COOH* was calculated at pH = 6.8 and U = −1.0 V_{RHE}. Since aminothiolate-coated Cu interface provides both the organic N and the inorganic Cu sites,[44] we examined both sites to activate CO_2. To differentiate, we used (Cu)−COOH* to denote the formation of COOH* at the Cu site and (NH)−COOH* to denote the formation of COOH* at the N site. The physical factors of ligand−metal interface, such as configuration, alkyl chain length, surface coverage, and Cu facet, were studied for the initial CO_2 activation.

Compared to the CO_2 activation on bare Cu(100), C_2 ligand at a low coverage (i.e., 1/16 ML) promotes the COOH* formation process in two ways (Figure 3a,b): (1) when CO_2 is activated at the Cu site, the hydrogen (H) bond from the amine group lowers (Cu)−COOH* formation by 0.13 eV (H-bond effect from the amine group is negligible when water is present in the model, which is discussed later in the section Solvation Effect); and (2) when CO_2 is activated at the N site, (NH)−COOH* formation can be promoted by 0.28 eV because the N−C bond has more electron transfer than the Cu−C bond.[44] Although it was pointed out earlier that C_2 at a coverage of 4/16 ML is 0.45 eV more favorable to form the flat-lying configuration rather than upright configuration on Cu(100) (Figure S1a), intermediates (e.g., CO*) during the CO_2RR could adsorb on Cu and compete for surface sites with the surface ligands. Thus, with the surface intermediates, ligands at 4/16 ML are more favorable to be the upright configurations. On the contrary, the intermediates do not influence the ligand configuration preference at a low coverage (i.e., 1/16 and 2/16 ML). At 4/16 ML, (Cu)−COOH* formation is not favorable on the Cu site because: (1) the amine group with the upright configuration is too far from the surface to induce the H-bond effect and thus to stabilize (Cu)−COOH* over the Cu site; (2) the strong lateral interaction from the high coverage of the ligands also destabilizes (Cu)−COOH* formation over the Cu sites. On the other hand, (NH)−COOH* formation at the N site at 4/16 ML is the most favorable among all the configurations due to the strong N−C bond and the H-bond formation between (NH)−COOH* and the adjacent amine group.[64]

To validate the aminothiolate ligand's ability to reactively capture and convert CO_2, we examined the formation energies of COOH* under different CO_2 surface coverages with and without the C_2 ligand. The examined surfaces included bare Cu(100), 1/16 ML of C_2/Cu(100), and 4/16 ML of C_2/Cu(100) (Figure S11). The energy diagram shown in Figure S12 suggests that (1) CO_2 activation over the Cu site (black line) is less favorable as compared to the scenarios with the C_2 ligand; (2) the N site of 1/16 ML C_2 ligand promotes the first CO_2 activation. The rest of CO_2 activate over the Cu sites and will not be influenced by the C_2 ligand (red line); and (3) 4/16 ML C_2 ligand promotes the first four CO_2 activation processes over the N sites. The fifth CO_2 activation over the Cu site is not as favorable as the ones over the N sites because of the surface lateral interaction from the adjacent ligands (blue line). However, the overall energy diagram of CO_2 activation over aminothiolate-coated Cu is much more thermodynamically

https://doi.org/10.1021/jacs.3c06888
J. Am. Chem. Soc. 2023, 145, 26038−26051

favorable than that over the bare Cu. These results prove that the aminothiolate ligand facilitates CO_2 reactive capture and conversion. As the ligand coverage increases, the potential capability of capturing and converting CO_2 is increased. In addition, the constructed first-principles Pourbaix diagrams for CO_2 activation with different CO_2 coverages over 1/16 ML (Figure S13) and 4/16 ML (Figure S14) C_2/Cu(100) indicate that at the neutral pH (the corresponding H-cell setup), lower applied potentials promote CO_2 activation over both the Cu and N sites.

We also examined the effects of the alkyl chain length on (NH)−COOH* formation at the N site (Figures 3c and S15). Our results show that for all alkyl chain lengths, the ligand−Cu interface with a coverage of 4/16 ML is always in favor of the (NH)−COOH* formation compared to that with 1/16 ML due to the hydrogen-bond formation between (NH)−COOH* and the adjacent amine group. The C_2, C_6, and C_{11} ligands at a coverage of 4/16 ML promote (NH)−COOH* formation by 0.41, 0.53, and 0.52 eV, respectively. This suggests that the ligands with longer alkyl chains (e.g., C_6 and C_{11}) are slightly more favorable for CO_2 activation than the ones with shorter lengths (e.g., C_2). Similar to Cu(100), aminothiolate ligands on Cu(111) can also favor COOH* (Figures S16 and S17). However, the aminothiolate with shorter alkyl chain lengths shows a better promoting effect for CO_2 activation. When CO_2 is activated at the N site, the C_2, C_6, and C_{11} ligands at a coverage of 4/16 ML enhance (NH)−COOH* formation by 1.17, 0.69, and 0.57 eV, respectively. This might be because longer ligands on the compact Cu(111) facet cause a robust repulsive effect on (NH)−COOH*, destabilizing its formation even with the hydrogen-bond effect. In summary, aminothiolate-coated Cu interface provides dual-active sites (Cu and N sites) to promote CO_2 activation via H and N−C bonds. The longer alkyl chain shows more favorable COOH* formation over the Cu(100) facet, while the shorter alkyl chain performs better over Cu(111).

C−C Coupling. C−C coupling (CO* + COH* → OCCOH* + *) is usually considered as the RDS of multicarbon products during CO_2RR (Scheme 1).[45,48,65] Our previous work has proven that COH* is more favorable at the N site, while CO* is more favorable at the Cu site.[44] We then calculated the role of ligand configuration and surface coverage effects of the ligand−metal interface on lowering the activation barrier of C−C coupling and thus enhancing the selectivity of multicarbon products (Figure 4a−d). The results show that C−C coupling on Cu(100) needs to overcome a high activation barrier of 0.89 eV. With the presence of 1/16 ML of C_2 ligand, CO* at the Cu site diffuses and binds to the COH* at the N site from the amine group. In this case, the activation barrier of C−C coupling decreases by 0.61 eV, meaning that C−C coupling becomes much more favorable with the C_2 ligand compared to the bare Cu. We attribute this enhancement to the dual organic−inorganic interfacial sites, that is, Cu and N sites, in enlarging the difference in adsorption energy between CO* and COH*, which is a descriptor for promoting C−C coupling.[46,53] We also measured other possible C−C coupling steps, that is, two-by-two combination between CO*, COH*, and CHO*,[66] over Cu(100) in the presence of 1/16 ML C_2 ligand. At the N site, both COH* and CHO* are stable, but CHO* cannot couple with another C species. Thus, for C−C coupling at the organic−inorganic interface, COH* is at the N site and couples with COH* and CHO* at the Cu site. Our results (Figure S18) show that for these two C−C coupling steps, that is, COH−COH and CHO−COH, dual organic−inorganic active sites still decrease the activation barriers by 0.2 and 0.59 eV compared to those over Cu(100), respectively.

The C−C coupling mechanism changes when the ligand surface coverage increases to 4/16 ML, where the ligand configurations are upright. Since COH* at the N site is far from the surface, OCCOH* is no longer formed near Cu. CO* first desorbs and overcomes a barrier of 0.77 eV to form the first transition state (TS1). Subsequently, CO* diffuses along the ligand until it is close to COH* at the tail of the ligand and then undergoes C−C coupling. For this scenario, the activation barrier required for the second transition state (TS2), that is, C−C coupling, is only 0.15 eV, which is lower than the activation barrier of C−C coupling at a low coverage of the ligands or over pure Cu. This is due to the formation of H bonds between OCCOH* and the adjacent amine group, which further stabilizes the adsorption of OCCOH*. To explore why TS1 needs a significant driving force for CO* desorption, we performed single-point calculations to investigate the interaction CO* receives during its upward movement (Figures S19−S21). The adsorption energy of CO* in the first initial state (IS1) is −0.23 eV. Since CO* leaves the surface, it receives a repulsive effect from the surface ligands at such a high coverage (i.e., 4/16 ML). The initial repulsion is large and then slowly decreases until it is coupled to COH* at the N site. In addition, the change of ligand configuration requires an energy of 0.16 eV before CO* desorption. Overall, three aspects, including the binding strength between Cu and CO*, the repulsion between CO* and the ligands, and the configuration change of the ligands, lead to a high barrier of 0.77 eV of CO* desorption and transportation of CO* before the C−C coupling.

We further compared the activation barrier of C−C coupling for longer ligands over Cu(100) (Figures 4e and S22, S23). At 4/16 ML, we only considered TS1, that is, the CO desorption step, because this step leads to a much higher barrier than the subsequent coupling step according to the earlier statement. The results indicate that the barrier of C−C coupling is alkyl chain length-independent at 1/16 ML with the flat-lying configuration. At 4/16 ML with the upright configuration, the barrier decreases as the alkyl chain length increases. This is because the lateral interaction induced by the long chain weakens the CO binding strength, making TS1 more favorable.

As for the post-C−C coupling steps, we found that OCCOH* formed at the dual site interface can move to the Cu surface for further reduction to ethylene/ethanol, as shown in Scheme 1, due to the energy favorability of the OCCOH* shift (Figure S24). Therefore, post-C−C coupling over the Cu surface in the presence of aminothiolate ligand performs similarly with that over bare Cu.[48,65] This means that the selectivity of the multicarbon product increases, while the ratio of ethylene/ethanol should remain similar between bare Cu and aminothiolate ligand-coated Cu. In addition, this energetic favorability of the OCCOH* shift also suggests that although the N site contributes to CO_2 activation and reduction, it is not poisoned by CO_2. After forming the (hydrogenated) CO dimer species via C−C coupling, further reduction to ethylene/ethanol will occur over the Cu sites, and thus, the aminothiolate ligand returns to its original state.

We measured the possible effect of the ligand on a single-carbon product (e.g., methane and methanol) by calculating the activation barrier of CHOH* formation (Figure S25),

https://doi.org/10.1021/jacs.3c06888
J. Am. Chem. Soc. 2023, 145, 26038−26051

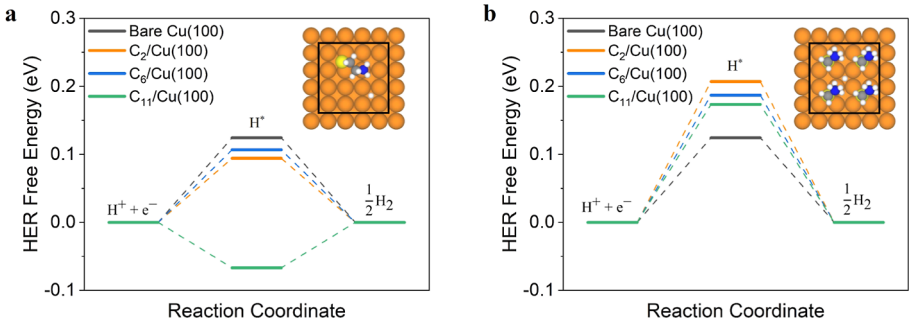

Figure 5. Free-energy diagram of HER on Cu(100) in the presence of aminothiolate ligands at coverages of (a) 1/16 and (b) 4/16 ML. The top view of H* adsorption is inserted. Color code refers to Figure 1.

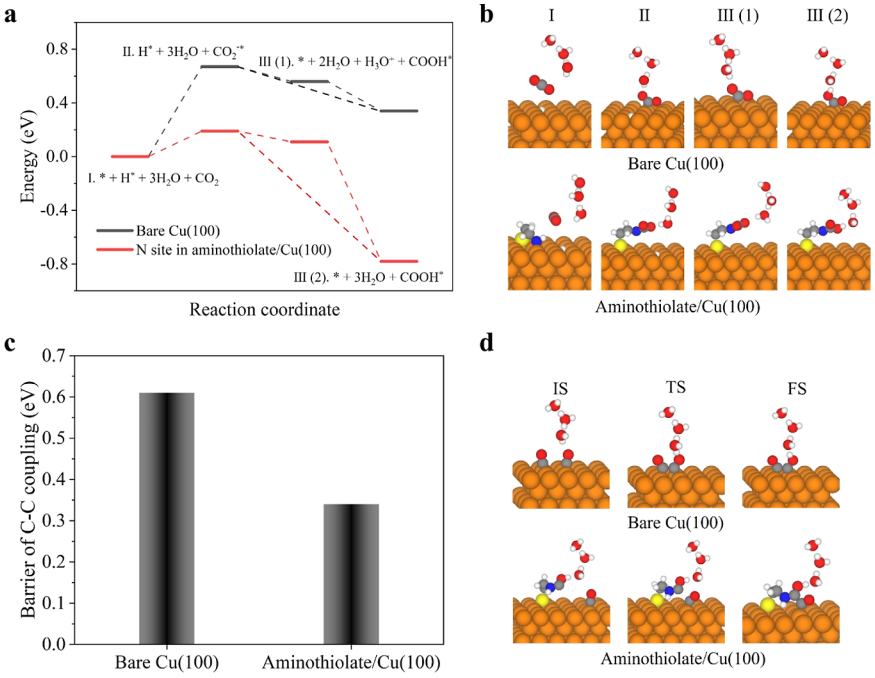

Figure 6. Solvation effect on CO_2 activation and C−C coupling over the N site of aminothiolate/Cu(100) and over the bare Cu(100) surface. (a) Energy diagram of CO_2 activation to form COOH* via surface H* and via proton transfer in the interfacial water layer; (b) optimized geometries of the steps in (a); (c) activation barrier of C−C coupling; and (d) optimized geometries of IS, TS, and FS during the coupling process in (c). Color code refers to Figure 3.

which is a key intermediate along CO_2-to-single-carbon product pathway.[47,65] The barriers are 0.99 and 0.39 eV when CHOH* forms at the Cu and N sites over aminothiolate/Cu(100). CHOH* formed over bare Cu(100) needs to overcome a barrier of 0.92 eV, suggesting that the presence of C_2 ligand suppresses CHOH* formation at the nearby Cu site but promotes CHOH* formation at the N site. However, the decreased barrier of CHOH* formation is still higher than the barrier of C−C coupling of 0.28 eV, indicating that the multicarbon product pathway is more favorable than the single-carbon product pathway.

Overall, the C−C coupling mechanism and performance are closely related to the alkyl chain length, ligand configuration, and surface coverage. When the ligands are flat-lying, C−C coupling is favorable both thermodynamically and kinetically compared with bare Cu. When the ligands are in an upright configuration, C−C coupling is not favorable kinetically. According to our earlier calculations regarding the ligand configurations, ligands with longer alkyl chain lengths occupy more surface sites, which make it difficult to form a flat-lying configuration even at a low surface coverage. Therefore, we expect that the aminothiolate ligand with shorter alkyl chain promotes C−C coupling more than the longer alkyl chain one.

Hydrogen Evolution Reaction. HER is a competitive reaction to CO_2RR and can theoretically be evaluated by the H* adsorption energy on the metal surface using the CHE model.[52] We measured the H* adsorption on Cu(100) and Cu(111) with various ligand alkyl chain lengths at the coverages of 1/16 and 4/16 ML and constructed the corresponding HER energy diagram (Figures 5 and S26). Our results show that the presence of the surface ligands at the coverage of 1/16 ML does not influence the HER significantly. When the coverage increases to 4/16 ML, HER can be suppressed on both Cu(100) and Cu(111) surfaces. Aminothiolates over Cu(111) have a better suppressing effect because the stronger lateral interactions between the ligands weaken the adsorption of H*. Three alkyl chain lengths have similar effects on suppressing the HER during CO_2RR. This demonstrates that once the protons in the solvent are transferred to the surface, their adsorption would not be

https://doi.org/10.1021/jacs.3c06888
J. Am. Chem. Soc. 2023, 145, 26038−26051

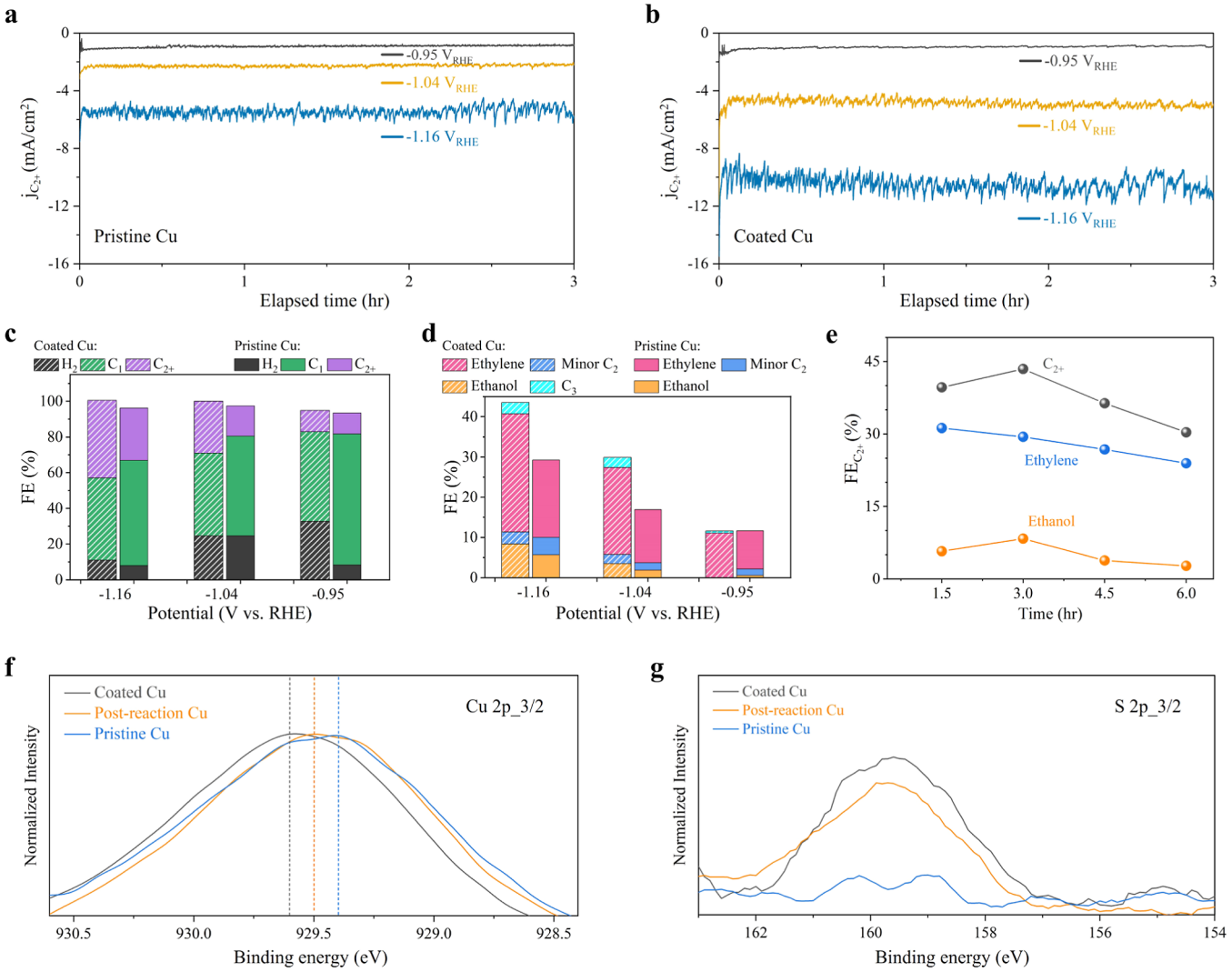

Figure 7. Experimental validation of surface ligand promotion on CO_2RR over Cu. (a) Partial current density of C_{2+} products over the pristine Cu; (b) partial current density of C_{2+} products over the coated Cu; (c) overall FE of C_{2+} products (ethanol, ethylene, acetic acid, acetaldehyde, and propionaldehyde), C_1 products (CO, CH_4, and formic acid), and H_2 over the coated and pristine Cu; (d) FE of individual C_{2+} products (minor C_2 products include acetic acid and acetaldehyde); (e) time-dependent FE of C_{2+} products; (f,g) XPS spectra of Cu $2p_{3/2}$ and S $2p_{3/2}$ for the fresh coated Cu, postreaction-coated Cu (under −1.16 V_{RHE}), and the pristine Cu.

affected by the alkyl chain length of the ligands. It is worth mentioning that our current work does not consider the transport of water, that is, how much water is close to the ligand−metal interface. Based on the literature review and the hydrophobicity of the thiolates with various alkyl chains, we expect that longer aminothiolate ligands could further suppress HER due to the fact that less water would transport near the ligand−Cu interface.[67]

Solvation Effect. All simulations performed so far were simplified using a gas/solid model. However, electrocatalytic CO_2 experiments are carried out under aqueous conditions. To incorporate the solvation and proton shuttling effects, we considered both the bulk water solvation using the implicit solvation model[68] combined with three explicit interface water molecules. We acknowledge that the hybrid solvation approach has limitations in simulating complex electrode/electrolyte interfaces. For example, the surface charge effect was not simulated here. When the negative potential is applied, the electrode surface is negatively charged. Due to the electrostatic attraction, the alkali cations become close to the electrode surface. Therefore, there will be a negative electric field effect on altering the energetics (adsorption, reaction, and activation barriers) of the reactions involving polarized intermediates, such as adsorbed CO_2, CO dimer, and the post C−C coupling species.[69−76] Such an electric field effect induced by the cations at the solid/liquid interface will be our future direction.

We investigated solvation and proton shuttling effects on both CO_2 activation and C−C coupling over bare Cu(100) and Cu(100) coated with a 1/16 ML C_2 ligand. For CO_2 activation at the N (Figure 6a,b) and Cu (Figure S27) sites, we followed the pathway:[77] (1) CO_2 adsorption to form CO_2^-* (I → II) and (2) proton transfer to form COOH* via surface H* (II → III (2)) or via proton shuttling in the interfacial water layers (II → III (1) → III (2)). Bader charge analysis indicates that after adsorption (I → II), CO_2 over bare Cu(100) is negatively charged (−0.8; Figure S28). In the presence of water, the N site provided by the C_2 ligand can decrease the energy requirement for CO_2 adsorption by 0.48 eV compared to bare Cu because of the strong N−C bond formation (Figure 6a,b). For proton transfer in the presence of water, the N site

https://doi.org/10.1021/jacs.3c06888
J. Am. Chem. Soc. 2023, 145, 26038−26051

provided by aminothiolate further lowered the energetics for CO_2^{-}* protonation to form COOH* by 1.12 eV compared to bare Cu (Figure 6a,b). When CO_2 is activated at the Cu site in the presence of water, the energetics of CO_2 activation are very similar with and without the surface aminothiolate (Figure S27). This suggests that when water is present, the H-bond effect from aminothiolate is negligible since COOH* is stabilized by the H bond from water.

For the C−C coupling over the N site (Figure 6c,d), we notice that COH* over the Cu site is unstable and that the H atom is shuttled between water layers. The activation barriers of C−C coupling over bare Cu(100) and C_2/Cu(100) are 0.63 and 0.32 eV, respectively. Thus, the N site provided by the C_2 ligand promotes C−C coupling over Cu(100) in the presence of water. Goddard's group[65] reported a barrier of 0.69 eV for C−C coupling over Cu(100) with solvation effects, which is similar to that of our result. Taking these together, our conclusion of CO_2 activation and C−C coupling promoted by organic−inorganic interfaces remains valid in the presence of the water effects (solvation and proton shuttling).

Experimental Validation. To validate the theoretical calculations and to study the effect of the aminothiolate ligand, we conducted an experimental study of the CO_2RR over the pristine and cysteamine ligand-coated Cu foil (denoted as coated Cu) under different applied potentials via a bath-type (H-cell) reactor. The average current density increases with increasing applied potentials. The coated Cu foil shows a higher current density than that of the pristine Cu at all tested potentials (Figure S29). The partial current density of multicarbon products (C_{2+}) is higher over the thiolate-coated Cu than the pristine Cu (Figure 7a,b). At −1.16 V_{RHE}, the partial current density of the C_{2+} product over the coated Cu is ∼10.5 mA/cm^2, which is 2-fold higher than that over the pristine Cu (5.5 mA/cm^2). The partial current density results show a consistent trend as the theoretical calculations.

Figures 7c and S30 show an overall Faradaic efficiency (FE) close to 100%, suggesting a good mass balance and a reliable setup for the CO_2RR electrocatalytic study. In addition, it is noted that the C_{2+} product selectivity is similar at a low applied potential (−0.95 V_{RHE}) for both electrodes. As the applied potential increased, the coated Cu exhibited a higher selectivity toward C_{2+} products than the pristine Cu. The highest C_{2+} product selectivity was found as 43% over the coated Cu electrode at −1.16 V_{RHE}, which is 1.5-fold higher than that for the pristine Cu (29%). Meanwhile, the formation of single-carbon (C_1) products was significantly suppressed by the coated Cu as the applied potential increased (Figure S31). Overall, the experimental product distribution is consistent with the theoretical calculations, that is, the deposit of aminothiolate ligand promotes C_{2+} products, while C_1 product formation over Cu catalyst is suppressed.

FE of individual C_{2+} products is shown in Figure 7d. We notice that the selectivity of C_{2+} products is enhanced under −1.04 and −1.16 V_{RHE}, but the ratio of ethylene/ethanol with and without the coated ligand is similar (Figure S32). This is consistent with the theoretical simulation showing the promotion of C−C coupling by the dual sites of amino-thiolate/Cu without affecting the post C−C coupling steps over the Cu site. It is worth mentioning that the coated Cu generates C_3 products under all three examined potentials, which cannot be observed with the pristine Cu catalyst. Electrochemical impedance spectroscopy (EIS) suggests that the coated Cu exhibited less limitation of mass transfer and smaller charge transfer impedance (Figure S33). Overall, the electrochemical results show that the aminothiolate ligand coating enhanced the catalytic activity for CO_2 reduction to multicarbon products over the Cu catalyst.

We further investigated the stability of the coated Cu catalyst under the optimal condition (i.e., −1.16 V_{RHE}) and the selectivity of each species (Figures 7e and S34). Our experiments show that the selectivity of the C_{2+} product over the coated Cu catalyst achieved a maximum value of 43% at 3 h and then decreased to 36% at 4.5 h and to 30% at 6 h. The C_{2+} product selectivity over the coated Cu catalyst at 6 h is still higher than that over the pristine Cu at 3 h (29%). Notably, ethylene selectivity decreased from 29% at 3 h to 27% (4.5 h) and to 24% (6 h), which are also higher than that of 19% over the pristine Cu (3 h). The ethanol selectivity over the coated Cu catalyst decreased from 8% (3 h) to 4% (4.5 h) and to 3% (6 h), which are slightly lower than the value of 6% over the pristine Cu (3 h). Considering the possible long-term catalytic deactivation of CO_2RR over the pristine Cu,[78−85] coating of aminothiolate was able to enhance the C_{2+} product selectivity for an extended reaction period. Additional discussion about the short reaction time (1.5 h) can be found in the Supporting Information (Figure S34).

To validate the existence of thiolate-type Cu−S, we applied X-ray photoelectron spectroscopy (XPS) to characterize the samples (Figures 7f,g and S35), including the pristine Cu, fresh coated Cu, and postreaction-coated Cu (under −1.16 V_{RHE}). The single peak of Cu $2p_{3/2}$ for the pristine Cu is referred to as Cu(0), which is near 929.3 eV (Figure 7f).[86,87] With the fresh coated Cu, the Cu $2p_{3/2}$ peak shifted to a higher energy state, suggesting a shift of oxidation state due to the thiolate-type Cu−S bond formation (shown in black dash line in Figure 7f). With the postreaction-coated Cu (under −1.16 V_{RHE}), the Cu $2p_{3/2}$ peak was in between the fresh coated Cu and pristine Cu. This suggests (1) the possible reductive desorption of thiolate SAMs from the fresh coated Cu surface during the CO_2RR, as predicted from the theory (Figures S5 and 2b); and (2) there are remaining thiolates over the postreaction-coated Cu. To illustrate that such shifts in the Cu $2p_{3/2}$ peak come from the thiolate-type Cu−S bond rather than oxygen poisoning, we also examined an oxidized Cu sample (Figure S35). The oxidized Cu presented a satellite peak at a much higher binding energy (931.6 eV, the typical peak of Cu(II)) than the peak (∼929.3 to ∼929.6 eV) of the thiolate-type Cu−S bond.[86,87]

The XPS results of S $2p_{3/2}$ are shown in Figure 7g. The coated Cu exhibited a S $2p_{3/2}$ peak around 160 eV,[86−92] indicating the attachment of thiolates, and there was no such S $2p_{3/2}$ peak in the pristine Cu sample.[86,87,90,91,93] After the reaction, the intensity of the $2p_{3/2}$ peak decreased slightly, suggesting the possible reductive desorption of thiolate SAMs from the fresh coated Cu surface during CO_2RR; however there were still plenty of remaining thiolates over the postreaction-coated Cu. This is consistent with the trend found in the Cu $2p_{3/2}$ results and theoretical prediction. In summary, the XPS results of the Cu $2p_{3/2}$ and S $2p_{3/2}$ peaks confirm the existence of the thiolate-type Cu−S bond in both fresh- and postreaction-coated Cu.

CONCLUSIONS

We performed DFT calculations to determine and quantify the role of ligand−metal interface on enhancing CO_2RR to multicarbon products, including the ligand−metal physical factors of configuration, surface coverage, dual organic−

https://doi.org/10.1021/jacs.3c06888
J. Am. Chem. Soc. 2023, 145, 26038−26051

inorganic sites, and facets. Flat-lying configuration is more favorable at a low surface coverage, while the upright configuration is more favorable at a high surface coverage. Aminothiolate with a longer alkyl chain is more stable due to more molecular interaction from the longer chain. The surface formation energy calculations indicate that coating surface ligands improves the catalyst stability under electrocatalysis conditions. The increased coverage of aminothiolate leads to the spontaneous reductive desorption of aminothiols into solvation. Thus, an optimal surface coverage of ≤1/4 ML was predicted by DFT.

As for the CO_2RR performance, the ligand−metal interface improves the activity of the CO_2RR (i.e., CO_2 activation to form COOH*) by the strong N−C bond from the amine group within the ligand. The selectivity of multicarbon products (i.e., C−C coupling) is enhanced by lowering the activation barriers up to ∼0.6 eV, through: (1) dual organic (N) and inorganic surface sites (Cu) at a low ligand coverage (i.e., flat-lying configuration); (2) strong C−N bond and H bond stabilizing the final product of C−C coupling at a high ligand coverage (i.e., upright configuration); (3) ligand-induced lateral interaction suppressing HER over the ligand−metal interface at a high ligand coverage. The ligand−metal interface returns to its original state after the post C−C coupling species, that is, OCCOH*, move to the Cu site for further reduction. The experiments validate the existence of a thiolate-type Cu−S bond before and after the CO_2RR using XPS spectra. The simulation conclusion was observed in an experiment study where both the selectivity and partial current density of C_{2+} products over the coated Cu catalysts were enhanced by 1.5-fold and 2-fold, respectively, without changing the ratio of ethylene/ethanol as compared to the pristine Cu at −1.16 V_{RHE}.

In summary, this detailed theoretical and experimental collaborative study determines and quantifies the key physical factors of the ligand−metal interface on tuning the stability, thermodynamic, and kinetic properties of CO_2 reactive capture and conversion. This work provides a theoretical basis for the future design of ligand-modulated catalysts. It also greatly advances the electrocatalysis field by introducing a new type of efficient and low-cost catalysts based on an interface between organic ligands and inorganic metal surface materials. This transformative concept—organic−inorganic dual interfacial sites—may be applied to other electrocatalytic reactions (e.g., ammonia synthesis and methane conversion) and thermal catalytic systems (e.g., SAM-assisted catalysis). Our future work will focus on establishing microkinetic modeling of CO_2RR over the ligand−metal interface under electrocatalytic working conditions, that is, using constant electrode potentials with grand canonical DFT,[94−99] and further validating with intensive experiments.

COMPUTATIONAL METHOD

DFT calculations were performed by Vienna ab initio simulation package (VASP).[100,101] The generalized gradient approximation[102] with the revised Perdew−Burke−Ernzerhof functional[103] was applied to treat exchange−correlation interactions. For the Ligand Stability sections, we implemented the optB88-vdW functional[104] to capture the long-term interaction between the ligands and obtained the most favorable ligand−metal interfacial geometries. For the remaining sections, we did not include the optB88-vdW functional because the van der Waals contributions overestimate the chemical binding strengths of the CO_2RR-related intermediate. An energy cutoff of 400 eV was used for the valence plane waves. The Cu lattice constant was calculated to be 3.68 Å. The Monkhorst−Pack mesh k-point grid of (3 × 3 × 1) was used for Cu(100) and Cu(111) facets with the supercell size of $p(4 \times 4)$. The Cu slab was constructed with four layers, where the bottom two layers were fixed to its bulk position, and two upper layers were relaxed. The examined surface−ligand model had an ∼15 Å vacuum separation between each periodic unit cell to avoid z-direction lateral interactions. Geometries were considered optimized when the energy had converged to 10^{-4} eV and the forces were smaller than 0.03 eV/Å. Regarding the low-frequency modes, we have reset the frequencies lower than 50 cm^{-1} to 50 cm^{-1} to avoid abnormal entropy contribution. Such treatment of low-frequency modes agrees with the current literature reports.[46,47]

The climbing image nudged elastic band[105] and dimer[106] methods were used to search for the transition state, which was further verified by calculating the vibrational frequencies, confirming that a single imaginary frequency was obtained. Transition-state geometries are converged at the energy level of 10^{-6} eV and at the force level of <0.05 eV/Å.

The implicit solvation model was applied to treat water as a continuum medium,[68] while explicit interface water molecules were added to incorporate the interaction between water and CO_2RR-related surface reactions. The previous report[94] has proven that such a combination of implicit and explicit solvation models could describe the CO_2RR performance well when compared with the experiments. More details about the calculations can be found in the Supporting Information.

EXPERIMENTAL METHOD

The experimental study of the CO_2RR was conducted via a bath-type (H-cell) reactor. The aminothiolate coating was applied on a Cu foil, via immersing the Cu foil into the aqueous solution of β-mercaptoethylamine hydrochloride. The Cu electrodes were analyzed via XPS measurements (PHI VersaProbe II Scanning XPS Microprobe) to identify the existence of the Cu−S bond. The CO_2RR was conducted over the coated and pristine Cu foils under several applied potentials. 0.1 M $KHCO_3$ was saturated with CO_2 for 30 min and used as the electrolyte with pH = 6.8. The products were collected after the electrolysis and analyzed via GC-TCD/FID for gas products and NMR for liquid products for determining the faradaic efficiency. Details regarding the coating process, electrochemical study, and CO_2RR product analysis are provided in the Supporting Information.

ASSOCIATED CONTENT

Supporting Information

The Supporting Information is available free of charge at https://pubs.acs.org/doi/10.1021/jacs.3c06888.

Computational and experimental setup details; geometries and energetics of ligands with various surface coverages and lengths over different Cu facets; more details of theoretical calculations of CO_2 activation, C−C coupling, and HER; details of experimental methods, catalyst synthesis, and XPS characterizations; and additional experimental results, e.g., FE of C_1 products and HER, total current density, EIS results, and XPS results (PDF)

https://doi.org/10.1021/jacs.3c06888
J. Am. Chem. Soc. 2023, 145, 26038−26051

AUTHOR INFORMATION

Corresponding Authors

Zhiyong Gu − *Department of Chemical Engineering, University of Massachusetts Lowell, Lowell, Massachusetts 01854, United States;* orcid.org/0000-0002-5613-4847; Email: zhiyong_gu@uml.edu

Fanglin Che − *Department of Chemical Engineering, University of Massachusetts Lowell, Lowell, Massachusetts 01854, United States;* orcid.org/0000-0001-5109-8296; Email: fanglin_che@uml.edu

Authors

Mingyu Wan − *Department of Chemical Engineering, University of Massachusetts Lowell, Lowell, Massachusetts 01854, United States*

Zhengyang Yang − *Department of Chemical Engineering, University of Massachusetts Lowell, Lowell, Massachusetts 01854, United States*

Heba Morgan − *Department of Chemical Engineering, University of Massachusetts Lowell, Lowell, Massachusetts 01854, United States*

Jinquan Shi − *Department of Electrical Engineering, Yale University, New Haven, Connecticut 06511, United States; Energy Sciences Institute, Yale University, West Haven, Connecticut 06520, United States*

Fan Shi − *National Energy Technology Laboratory, Pittsburgh, Pennsylvania 15236, United States;* orcid.org/0000-0002-2738-9920

Mengxia Liu − *Department of Electrical Engineering, Yale University, New Haven, Connecticut 06511, United States; Energy Sciences Institute, Yale University, West Haven, Connecticut 06520, United States*

Hsi-Wu Wong − *Department of Chemical Engineering, University of Massachusetts Lowell, Lowell, Massachusetts 01854, United States;* orcid.org/0000-0003-2623-6145

Complete contact information is available at: https://pubs.acs.org/10.1021/jacs.3c06888

Author Contributions

⊥M.W. and Z.Y. contributed equally.

Notes

The authors declare no competing financial interest.

ACKNOWLEDGMENTS

M.W., Z.Y., Z.G., and F.C. acknowledge the support from National Science Foundation with award number 2103478. F.C. also thanks the support provided by Department of Energy, Basic Energy Science, Catalysis Science, Early Career Research Program under the award number of DE-SC0024553, for the support. M.W. and F.C. thank the computational resources at Massachusetts Green High Performance Computing Center (MGHPCC). M.W. and F.C. thank the San Diego Supercomputer Center at University of California San Diego through allocation no. CHM220016, no. CHE200083, and no. CHE220075 from the Advanced Cyberinfrastructure Coordination Ecosystem: Services & Support (ACCESS) program, which is supported by National Science Foundation grants # 2103478.[107] M.L. and J.S. acknowledge the support from Yale faculty start-up and the help from Min Li at Yale Materials Characterization Core. The authors further acknowledge Jason Guinan (NETL Multimedia Team) for the design of the cover art.

REFERENCES

(1) Davis, S. J.; Caldeira, K.; Matthews, H. D. Future CO_2 emissions and climate change from existing energy infrastructure. *Science* **2010**, *329*, 1330−1333.

(2) Barlow, J. M.; Yang, J. Y. Oxygen-stable electrochemical CO_2 capture and concentration with quinones using alcohol additives. *J. Am. Chem. Soc.* **2022**, *144*, 14161−14169.

(3) Zito, A. M.; Bím, D.; Vargas, S.; Alexandrova, A. N.; Yang, J. Y. Computational and experimental design of quinones for electrochemical CO_2 capture and concentration. *ACS Sustain. Chem. Eng.* **2022**, *10*, 11387−11395.

(4) Shafaat, H. S.; Yang, J. Y. Uniting biological and chemical strategies for selective CO_2 reduction. *Nat. Catal.* **2021**, *4*, 928−933.

(5) Zito, A. M.; Clarke, L. E.; Barlow, J. M.; Bím, D.; Zhang, Z.; Ripley, K. M.; Li, C.; Kummeth, A.; Leonard, M. E.; Alexandrova, A. N.; Brushett, F. R.; Yang, J. Y. Electrochemical carbon dioxide capture and concentration. *Chem. Rev.* **2023**, *123*, 8069−8098.

(6) Proppe, A. H.; Li, Y. C.; Aspuru-Guzik, A.; Berlinguette, C. P.; Chang, C. J.; Cogdell, R.; Doyle, A. G.; Flick, J.; Gabor, N. M.; van Grondelle, R.; Hammes-Schiffer, S.; Jaffer, S. A.; Kelley, S. O.; Leclerc, M.; Leo, K.; Mallouk, T. E.; Narang, P.; Schlau-Cohen, G. S.; Scholes, G. D.; Vojvodic, A.; Yam, V. W.-W.; Yang, J. Y.; Sargent, E. H. Bioinspiration in light harvesting and catalysis. *Nat. Rev. Mater.* **2020**, *5*, 828−846.

(7) Poliakoff, M.; Leitner, W.; Streng, E. S. The twelve principles of CO_2 CHEMISTRY. *Faraday Discuss.* **2015**, *183*, 9−17.

(8) Shi, J.; Jiang, Y.; Jiang, Z.; Wang, X.; Wang, X.; Zhang, S.; Han, P.; Yang, C. Enzymatic conversion of carbon dioxide. *Chem. Soc. Rev.* **2015**, *44*, 5981−6000.

(9) Roy, S.; Cherevotan, A.; Peter, S. C. Thermochemical CO_2 hydrogenation to single carbon products: Scientific and technological challenges. *ACS Energy Lett.* **2018**, *3*, 1938−1966.

(10) Birdja, Y. Y.; Pérez-Gallent, E.; Figueiredo, M. C.; Göttle, A. J.; Calle-Vallejo, F.; Koper, M. T. M. Advances and challenges in understanding the electrocatalytic conversion of carbon dioxide to fuels. *Nat. Energy* **2019**, *4*, 732−745.

(11) Ran, J.; Jaroniec, M.; Qiao, S. Z. Cocatalysts in semiconductor-based photocatalytic CO_2 reduction: Achievements, challenges, and opportunities. *Adv. Mater.* **2018**, *30*, 1704649.

(12) Schreier, M.; Luo, J.; Gao, P.; Moehl, T.; Mayer, M. T.; Gratzel, M. Covalent immobilization of a molecular catalyst on Cu_2O photocathodes for CO_2 reduction. *J. Am. Chem. Soc.* **2016**, *138*, 1938−1946.

(13) Ong, M. Y.; Nomanbhay, S.; Kusumo, F.; Show, P. L. Application of microwave plasma technology to convert carbon dioxide (CO_2) into high value products: A review. *J. Clean. Prod.* **2022**, *336*, 130447.

(14) Ji, T.; Zhai, H.; Wang, C.; Culp, J.; Marin, C. M.; Paudel, H. P.; Wilfong, W. C.; Duan, Y.; Xia, R.; Jiao, F.; Kail, B.; Wang, Q.; Soong, Y.; Shi, F.; Gray, M. Microwave-accelerated regeneration of a non-aqueous slurry for energy-efficient carbon sequestration. *Mater. Today Sustain.* **2022**, *19*, 100168.

(15) Jouny, M.; Luc, W.; Jiao, F. General techno-economic analysis of CO_2 electrolysis systems. *Ind. Eng. Chem. Res.* **2018**, *57*, 2165−2177.

(16) Nitopi, S.; Bertheussen, E.; Scott, S. B.; Liu, X.; Engstfeld, A. K.; Horch, S.; Seger, B.; Stephens, I. E. L.; Chan, K.; Hahn, C.; Norskov, J. K.; Jaramillo, T. F.; Chorkendorff, I. Progress and perspectives of electrochemical CO_2 reduction on copper in aqueous electrolyte. *Chem. Rev.* **2019**, *119*, 7610−7672.

(17) De Luna, P.; Hahn, C.; Higgins, D.; Jaffer, S. A.; Jaramillo, T. F.; Sargent, E. H. What would it take for renewably powered electrosynthesis to displace petrochemical processes? *Science* **2019**, *364*, 350.

(18) Love, J. C.; Estroff, L. A.; Kriebel, J. K.; Nuzzo, R. G.; Whitesides, G. M. Self-assembled monolayers of thiolates on metals as a form of nanotechnology. *Chem. Rev.* **2005**, *105*, 1103−1170.

(19) Liu, P.; Qin, R.; Fu, G.; Zheng, N. Surface coordination chemistry of metal nanomaterials. *J. Am. Chem. Soc.* **2017**, *139*, 2122−2131.
(20) Marshall, S. T.; O'Brien, M.; Oetter, B.; Corpuz, A.; Richards, R. M.; Schwartz, D. K.; Medlin, J. W. Controlled selectivity for palladium catalysts using self-assembled monolayers. *Nat. Mater.* **2010**, *9*, 853−858.
(21) Pang, S. H.; Schoenbaum, C. A.; Schwartz, D. K.; Medlin, J. W. Directing reaction pathways by catalyst active-site selection using self-assembled monolayers. *Nat. Commun.* **2013**, *4*, 2448.
(22) Mark, L. O.; Zhu, C.; Medlin, J. W.; Heinz, H. Understanding the surface reactivity of ligand-protected metal nanoparticles for biomass upgrading. *ACS Catal.* **2020**, *10*, 5462−5474.
(23) Chen, G.; Xu, C.; Huang, X.; Ye, J.; Gu, L.; Li, G.; Tang, Z.; Wu, B.; Yang, H.; Zhao, Z.; Zhou, Z.; Fu, G.; Zheng, N. Interfacial electronic effects control the reaction selectivity of platinum catalysts. *Nat. Mater.* **2016**, *15*, 564−569.
(24) Ellis, L. D.; Trottier, R. M.; Musgrave, C. B.; Schwartz, D. K.; Medlin, J. W. Controlling the surface reactivity of titania via electronic tuning of self-assembled monolayers. *ACS Catal.* **2017**, *7*, 8351−8357.
(25) Zhu, Q.; Murphy, C. J.; Baker, L. R. Opportunities for electrocatalytic CO_2 reduction enabled by surface ligands. *J. Am. Chem. Soc.* **2022**, *144*, 2829−2840.
(26) Yu, S.; Louisia, S.; Yang, P. The interactive dynamics of nanocatalyst structure and microenvironment during electrochemical CO_2 conversion. *JACS Au* **2022**, *2*, 562−572.
(27) Li, Y.; Xu, A.; Lum, Y.; Wang, X.; Hung, S. F.; Chen, B.; Wang, Z.; Xu, Y.; Li, F.; Abed, J.; Huang, J. E.; Rasouli, A. S.; Wicks, J.; Sagar, L. K.; Peng, T.; Ip, A. H.; Sinton, D.; Jiang, H.; Li, C.; Sargent, E. H. Promoting CO_2 methanation via ligand-stabilized metal oxide clusters as hydrogen-donating motifs. *Nat. Commun.* **2020**, *11*, 6190.
(28) Pankhurst, J. R.; Iyengar, P.; Loiudice, A.; Mensi, M.; Buonsanti, R. Metal-ligand bond strength determines the fate of organic ligands on the catalyst surface during the electrochemical CO_2 reduction reaction. *Chem. Sci.* **2020**, *11*, 9296−9302.
(29) Kim, D.; Yu, S.; Zheng, F.; Roh, I.; Li, Y.; Louisia, S.; Qi, Z.; Somorjai, G. A.; Frei, H.; Wang, L.-W.; Yang, P. Selective CO_2 electrocatalysis at the pseudocapacitive nanoparticle/ordered-ligand interlayer. *Nat. Energy* **2020**, *5*, 1032−1042.
(30) Banerjee, S.; Zhang, Z.-Q.; Hall, A. S.; Thoi, V. S. Surfactant perturbation of cation interactions at the electrode-electrolyte interface in carbon dioxide reduction. *ACS Catal.* **2020**, *10*, 9907−9914.
(31) Banerjee, S.; Han, X.; Thoi, V. S. Modulating the electrode-electrolyte interface with cationic surfactants in carbon dioxide reduction. *ACS Catal.* **2019**, *9*, 5631−5637.
(32) Lee, G.; Li, Y. C.; Kim, J.-Y.; Peng, T.; Nam, D.-H.; Sedighian Rasouli, A.; Li, F.; Luo, M.; Ip, A. H.; Joo, Y.-C.; Sargent, E. H. Electrochemical upgrade of CO_2 from amine capture solution. *Nat. Energy* **2021**, *6*, 46−53.
(33) Khatri, R. A.; Chuang, S. S. C.; Soong, Y.; Gray, M. Thermal and chemical stability of regenerable solid amine sorbent for CO_2 capture. *Energy Fuels* **2006**, *20*, 1514−1520.
(34) Shen, X.; Du, H.; Mullins, R. H.; Kommalapati, R. R. Polyethylenimine applications in carbon dioxide capture and separation: From theoretical study to experimental work. *Energy Technol.* **2017**, *5*, 822−833.
(35) Barlow, J. M.; Clarke, L. E.; Zhang, Z.; Bím, D.; Ripley, K. M.; Zito, A.; Brushett, F. R.; Alexandrova, A. N.; Yang, J. Y. Molecular design of redox carriers for electrochemical CO_2 capture and concentration. *Chem. Soc. Rev.* **2022**, *51*, 8415−8433.
(36) Wang, Z.; Wu, L.; Sun, K.; Chen, T.; Jiang, Z.; Cheng, T.; Goddard, W. A. Surface ligand promotion of carbon dioxide reduction through stabilizing chemisorbed reactive intermediates. *J. Phys. Chem. Lett.* **2018**, *9*, 3057−3061.
(37) Wang, Z.; Sun, K.; Liang, C.; Wu, L.; Niu, Z.; Gao, J. Synergistic chemisorbing and electronic effects for efficient CO_2 reduction using cysteamine-functionalized gold nanoparticles. *ACS Appl. Energy Mater.* **2019**, *2*, 192−195.
(38) Bai, X.; Shi, L.; Li, Q.; Ling, C.; Ouyang, Y.; Wang, S.; Wang, J. Synergistic effect of metal doping and tethered ligand promoted high-selectivity conversion of CO_2 to C_2 oxygenates at ultra-low potential. *Energy Environ. Mater.* **2022**, *5*, 892−898.
(39) Zhang, J.; Deo, S.; Janik, M. J.; Medlin, J. W. Control of molecular bonding strength on metal catalysts with organic monolayers for CO_2 reduction. *J. Am. Chem. Soc.* **2020**, *142*, 5184−5193.
(40) Fang, Y.; Flake, J. C. Electrochemical reduction of CO_2 at functionalized Au electrodes. *J. Am. Chem. Soc.* **2017**, *139*, 3399−3405.
(41) Li, F.; Tang, Q. Understanding the role of functional groups of thiolate ligands in electrochemical CO_2 reduction over Au(111) from first-principles. *J. Mater. Chem. A* **2019**, *7*, 19872−19880.
(42) Yang, Z.; Wan, M.; Gu, Z.; Che, F. Zhiyong Gu, Fanglin Che, CO_2RR-to-CO enhanced by self-assembled monolayer and Ag catalytic interface. *J. Phys. Chem. C* **2023**, *127*, 17685−17693.
(43) Sandru, M.; Sandru, E. M.; Ingram, W. F.; Deng, J.; Stenstad, P. M.; Deng, L.; Spontak, R. J. An integrated materials approach to ultrapermeable and ultraselective CO_2 polymer membranes. *Science* **2022**, *376*, 90−94.
(44) Wan, M.; Gu, Z.; Che, F. Hybrid organic-inorganic heterogeneous interfaces for electrocatalysis: A theoretical study of CO_2 reduction to C_2. *ChemCatChem* **2022**, *14*, No. e202101224.
(45) Kortlever, R.; Shen, J.; Schouten, K. J.; Calle-Vallejo, F.; Koper, M. T. Catalysts and reaction pathways for the electrochemical reduction of carbon dioxide. *J. Phys. Chem. Lett.* **2015**, *6*, 4073−4082.
(46) Xiao, H.; Goddard, W. A.; Cheng, T.; Liu, Y. Cu metal embedded in oxidized matrix catalyst to promote CO_2 activation and CO dimerization for electrochemical reduction of CO_2. *Proc. Natl. Acad. Sci. U.S.A.* **2017**, *114*, 6685−6688.
(47) Xiao, H.; Cheng, T.; Goddard, W. A. Atomistic mechanisms underlying selectivities in C_1 and C_2 products from electrochemical reduction of CO on Cu(111). *J. Am. Chem. Soc.* **2017**, *139*, 130−136.
(48) Lum, Y.; Cheng, T.; Goddard, W. A.; Ager, J. W. Electrochemical CO reduction builds solvent water into oxygenate products. *J. Am. Chem. Soc.* **2018**, *140*, 9337−9340.
(49) Maksymovych, P.; Sorescu, D. C.; Yates, J. T. Gold-adatom-mediated bonding in self-assembled short-chain alkanethiolate species on the Au(111) surface. *Phys. Rev. Lett.* **2006**, *97*, 146103.
(50) Clerix, J. J.; Sanz-Matias, A.; Armini, S.; Harvey, J. N.; Delabie, A. Structural phases of alkanethiolate self-assembled monolayers (C1−12) on Cu[100] by density functional theory. *J. Phys. Chem. C* **2020**, *124*, 3802−3811.
(51) Lahann, J.; Mitragotri, S.; Tran, T.-N.; Kaido, H.; Sundaram, J.; Choi, I. S.; Hoffer, S.; Somorjai, G. A.; Langer, R. A reversibly switching surface. *Science* **2003**, *299*, 371−374.
(52) Nørskov, J. K.; Bligaard, T.; Logadottir, A.; Kitchin, J. R.; Chen, J. G.; Pandelov, S.; Stimming, U. Trends in the exchange current for hydrogen evolution. *J. Electrochem. Soc.* **2005**, *152*, J23.
(53) Zhou, Y.; Che, F.; Liu, M.; Zou, C.; Liang, Z.; De Luna, P.; Yuan, H.; Li, J.; Wang, Z.; Xie, H.; Li, H.; Chen, P.; Bladt, E.; Quintero-Bermudez, R.; Sham, T. K.; Bals, S.; Hofkens, J.; Sinton, D.; Chen, G.; Sargent, E. H. Dopant-induced electron localization drives CO_2 reduction to C_2 hydrocarbons. *Nat. Chem.* **2018**, *10*, 974−980.
(54) Schwartz, D. K. Mechanisms and kinetics of self-assembled monolayer formation. *Annu. Rev. Phys. Chem.* **2001**, *52*, 107−137.
(55) Salvarezza, R. C.; Carro, P. The electrochemical stability of thiols on gold surfaces. *J. Electroanal. Chem.* **2018**, *819*, 234−239.
(56) Ramos, N. C.; Medlin, J. W.; Holewinski, A. Electrochemical stability of thiolate self-assembled monolayers on Au, Pt, and Cu. *ACS Appl. Mater. Interfaces* **2023**, *15*, 14470−14480.
(57) Bedford, E.; Humblot, V.; Methivier, C.; Pradier, C. M.; Gu, F.; Tielens, F.; Boujday, S. An experimental and theoretical approach to investigate the effect of chain length on aminothiol adsorption and assembly on gold. *Chemistry* **2015**, *21*, 14555−14561.
(58) Truyens, A.-J.; Vekeman, J.; Tielens, F. A subtle balance between interchain interactions and surface reconstruction at the

https://doi.org/10.1021/jacs.3c06888
J. Am. Chem. Soc. 2023, 145, 26038−26051

origin of the alkylthiol/Au(111) self-assembled monolayer geometry. *Surf. Sci.* **2020**, *696*, 121597.
(59) Floridia Addato, M. A.; Rubert, A. A.; Benítez, G. A.; Fonticelli, M. H.; Carrasco, J.; Carro, P.; Salvarezza, R. C. Alkanethiol adsorption on platinum: Chain length effects on the quality of self-assembled monolayers. *J. Phys. Chem. C* **2011**, *115*, 17788−17798.
(60) Rechmann, J.; Krzywiecki, M.; Erbe, A. Carbon-sulfur bond cleavage during adsorption of octadecane thiol to copper in ethanol. *Langmuir* **2019**, *35*, 6888−6897.
(61) Love, J. C.; Wolfe, D. B.; Haasch, R.; Chabinyc, M. L.; Paul, K. E.; Whitesides, G. M.; Nuzzo, R. G. Formation and structure of self-assembled monolayers of alkanethiolates on palladium. *J. Am. Chem. Soc.* **2003**, *125*, 2597−2609.
(62) Logadottir, A.; Rod, T. H.; Nørskov, J.; Hammer, B.; Dahl, S.; Jacobsen, C. J. H. The Brønsted−Evans−Polanyi relation and the volcano plot for ammonia synthesis over transition metal catalysts. *J. Catal.* **2001**, *197*, 229−231.
(63) Wang, S.; Temel, B.; Shen, J.; Jones, G.; Grabow, L. C.; Studt, F.; Bligaard, T.; Abild-Pedersen, F.; Christensen, C. H.; Nørskov, J. K. Universal Brønsted-Evans-Polanyi relations for C−C, C−O, C−N, N−O, N−N, and O−O dissociation reactions. *Catal. Lett.* **2011**, *141*, 370−373.
(64) Xiao, J.; Sitamraju, S.; Janik, M. J. CO_2 adsorption thermodynamics over n-substituted/grafted graphanes: A DFT study. *Langmuir* **2014**, *30*, 1837−1844.
(65) Cheng, T.; Xiao, H.; Goddard, W. A. Full atomistic reaction mechanism with kinetics for CO reduction on Cu(100) from ab initio molecular dynamics free-energy calculations at 298 k. *Proc. Natl. Acad. Sci. U.S.A.* **2017**, *114*, 1795−1800.
(66) Zhao, Q.; Martirez, J. M. P.; Carter, E. A. Charting C-C coupling pathways in electrochemical CO_2 reduction on Cu(111) using embedded correlated wavefunction theory. *Proc. Natl. Acad. Sci. U.S.A.* **2022**, *119*, No. e2202931119.
(67) Pankhurst, J. R.; Guntern, Y. T.; Mensi, M.; Buonsanti, R. Molecular tunability of surface-functionalized metal nanocrystals for selective electrochemical CO_2 reduction. *Chem. Sci.* **2019**, *10*, 10356−10365.
(68) Mathew, K.; Sundararaman, R.; Letchworth-Weaver, K.; Arias, T. A.; Hennig, R. G. Implicit solvation model for density-functional study of nanocrystal surfaces and reaction pathways. *J. Chem. Phys.* **2014**, *140*, 084106.
(69) Chen, L. D.; Urushihara, M.; Chan, K.; Nørskov, J. K. Electric field effects in electrochemical CO_2 reduction. *ACS Catal.* **2016**, *6*, 7133−7139.
(70) Resasco, J.; Chen, L. D.; Clark, E.; Tsai, C.; Hahn, C.; Jaramillo, T. F.; Chan, K.; Bell, A. T. Promoter effects of alkali metal cations on the electrochemical reduction of carbon dioxide. *J. Am. Chem. Soc.* **2017**, *139*, 11277−11287.
(71) Sharifi Golru, S.; Biddinger, E. J. Effect of additives in aqueous electrolytes on CO_2 electroreduction. *J. Chem. Eng.* **2022**, *428*, 131303.
(72) Waegele, M. M.; Gunathunge, C. M.; Li, J.; Li, X. How cations affect the electric double layer and the rates and selectivity of electrocatalytic processes. *J. Chem. Phys.* **2019**, *151*, 160902.
(73) Li, X.; Gunathunge, C. M.; Agrawal, N.; Montalvo-Castro, H.; Jin, J.; Janik, M. J.; Waegele, M. M. Impact of alkali metal cations and iron impurities on the evolution of hydrogen on Cu electrodes in alkaline electrolytes. *J. Electrochem. Soc.* **2020**, *167*, 106505.
(74) Cheng, T.; Fortunelli, A.; Goddard, W. A. Reaction intermediates during operando electrocatalysis identified from full solvent quantum mechanics molecular dynamics. *Proc. Natl. Acad. Sci. U.S.A.* **2019**, *116*, 7718−7722.
(75) Ovalle, V. J.; Hsu, Y. S.; Agrawal, N.; Janik, M. J.; Waegele, M. M. Correlating hydration free energy and specific adsorption of alkali metal cations during CO_2 electroreduction on Au. *Nat. Catal.* **2022**, *5*, 624−632.
(76) Estejab, A.; Garcia Carcamo, R. A.; Getman, R. B. Influence of an electrified interface on the entropy and energy of solvation of methanol oxidation intermediates on platinum(111) under explicit solvation. *Phys. Chem. Chem. Phys.* **2022**, *24*, 4251−4261.
(77) Nie, X.; Luo, W.; Janik, M. J.; Asthagiri, A. Reaction mechanisms of CO_2 electrochemical reduction on Cu(111) determined with density functional theory. *J. Catal.* **2014**, *312*, 108−122.
(78) Nitopi, S.; Bertheussen, E.; Scott, S. B.; Liu, X.; Engstfeld, A. K.; Horch, S.; Seger, B.; Stephens, I. E. L.; Chan, K.; Hahn, C.; Norskov, J. K.; Jaramillo, T. F.; Chorkendorff, I. Progress and perspectives of electrochemical CO_2 reduction on copper in aqueous electrolyte. *Chem. Rev.* **2019**, *119*, 7610−7672.
(79) Yang, C.-H.; Nosheen, F.; Zhang, Z.-C. Recent progress in structural modulation of metal nanomaterials for electrocatalytic CO_2 reduction. *Rare Met.* **2021**, *40*, 1412−1430.
(80) Woldu, A. R.; Huang, Z.; Zhao, P.; Hu, L.; Astruc, D. Electrochemical CO_2 reduction (CO_2RR) to multi-carbon products over copper-based catalysts. *Coord. Chem. Rev.* **2022**, *454*, 214340.
(81) Tabassum, H.; Yang, X.; Zou, R.; Wu, G. Surface engineering of Cu catalysts for electrochemical reduction of CO_2 to value-added multi-carbon products. *Chem Catal.* **2022**, *2*, 1561−1593.
(82) Liu, M.; Pang, Y.; Zhang, B.; De Luna, P.; Voznyy, O.; Xu, J.; Zheng, X.; Dinh, C. T.; Fan, F.; Cao, C.; de Arquer, F. P. G.; Safaei, T. S.; Mepham, A.; Klinkova, A.; Kumacheva, E.; Filleter, T.; Sinton, D.; Kelley, S. O.; Sargent, E. H. Enhanced electrocatalytic CO_2 reduction via field-induced reagent concentration. *Nature* **2016**, *537*, 382−386.
(83) Huang, P.; Ci, S.; Wang, G.; Jia, J.; Xu, J.; Wen, Z. High-activity Cu nanowires electrocatalysts for CO_2 reduction. *J. CO_2 Util.* **2017**, *20*, 27−33.
(84) Heenan, A. R.; Hamonnet, J.; Marshall, A. T. Why careful iR compensation and reporting of electrode potentials are critical for the CO_2 reduction reaction. *ACS Energy Lett.* **2022**, *7*, 2357−2361.
(85) Garg, S.; Li, M.; Weber, A. Z.; Ge, L.; Li, L.; Rudolph, V.; Wang, G.; Rufford, T. E. Advances and challenges in electrochemical CO_2 reduction processes: An engineering and design perspective looking beyond new catalyst materials. *J. Mater. Chem. A* **2020**, *8*, 1511−1544.
(86) Laibinis, P. E.; Whitesides, G. M. Self-assembled monolayers of n-alkanethiolates on copper are barrier films that protect the metal against oxidation by air. *J. Am. Chem. Soc.* **1992**, *114*, 9022−9028.
(87) Laibinis, P. E.; Whitesides, G. M.; Allara, D. L.; Tao, Y. T.; Parikh, A. N.; Nuzzo, R. G. Comparison of the structures and wetting properties of self-assembled monolayers of n-alkanethiols on the coinage metal surfaces, copper, silver, and gold. *J. Am. Chem. Soc.* **1991**, *113*, 7152−7167.
(88) Schoenfisch, M. H.; Pemberton, J. E. Air stability of alkanethiol self-assembled monolayers on silver and gold surfaces. *J. Am. Chem. Soc.* **1998**, *120*, 4502−4513.
(89) Kumar, S.; Soni, S.; Danowski, W.; van Beek, C. L. F.; Feringa, B. L.; Rudolf, P.; Chiechi, R. C. Correlating the influence of disulfides in monolayers across photoelectron spectroscopy wettability and tunneling charge-transport. *J. Am. Chem. Soc.* **2020**, *142*, 15075−15083.
(90) Jennings, G. K.; Munro, J. C.; Yong, T.-H.; Laibinis, P. E. Effect of chain length on the protection of copper by n-alkanethiols. *Langmuir* **1998**, *14*, 6130−6139.
(91) Jennings, G. K.; Yong, T.-H.; Munro, J. C.; Laibinis, P. E. Structural effects on the barrier properties of self-assembled monolayers formed from long-chain ω-alkoxy-n-alkanethiols on copper. *J. Am. Chem. Soc.* **2003**, *125*, 2950−2957.
(92) Ulman, A. Formation and structure of self-assembled monolayers. *Chem. Rev.* **1996**, *96*, 1533−1554.
(93) Sung, M. M.; Sung, K.; Kim, C. G.; Lee, S. S.; Kim, Y. Self-assembled monolayers of alkanethiols on oxidized copper surfaces. *J. Phys. Chem. B* **2000**, *104*, 2273−2277.
(94) Goodpaster, J. D.; Bell, A. T.; Head-Gordon, M. Identification of possible pathways for C-C bond formation during electrochemical reduction of CO_2: New theoretical insights from an improved electrochemical model. *J. Phys. Chem. Lett.* **2016**, *7*, 1471−1477.

(95) Garza, A. J.; Bell, A. T.; Head-Gordon, M. Mechanism of CO_2 reduction at copper surfaces: Pathways to C_2 products. *ACS Catal.* **2018**, *8*, 1490−1499.
(96) Pillai, H. S.; Xin, H. New insights into electrochemical ammonia oxidation on Pt(100) from first principles. *Ind. Eng. Chem. Res.* **2019**, *58*, 10819−10828.
(97) Zhao, X.; Levell, Z. H.; Yu, S.; Liu, Y. Atomistic understanding of two-dimensional electrocatalysts from first principles. *Chem. Rev.* **2022**, *122*, 10675−10709.
(98) Akhade, S. A.; Bernstein, N. J.; Esopi, M. R.; Regula, M. J.; Janik, M. J. A simple method to approximate electrode potential-dependent activation energies using density functional theory. *Catal. Today* **2017**, *288*, 63−73.
(99) Sundararaman, R.; Goddard, W. A.; Arias, T. A. Grand canonical electronic density-functional theory: Algorithms and applications to electrochemistry. *J. Chem. Phys.* **2017**, *146*, 114104.
(100) Kresse, G.; Hafner, J. Ab initio molecular dynamics for liquid metals. *Phys. Rev. B: Condens. Matter Mater. Phys.* **1993**, *47*, 558−561.
(101) Kresse, G.; Furthmüller, J. Efficiency of ab-initio total energy calculations for metals and semiconductors using a plane-wave basis set. *Comput. Mater. Sci.* **1996**, *6*, 15−50.
(102) Perdew, J.; Burke, K.; Ernzerhof, M. Generalized gradient approximation made simple. *Phys. Rev. Lett.* **1996**, *77*, 3865−3868.
(103) Hammer, B.; Hansen, L. B.; Nørskov, J. K. Improved adsorption energetics within density-functional theory using revised Perdew-Burke-Ernzerhof functionals. *Phys. Rev. B: Condens. Matter Mater. Phys.* **1999**, *59*, 7413−7421.
(104) Klimeš, J.; Bowler, D. R.; Michaelides, A. Van der Waals density functionals applied to solids. *Phys. Rev. B: Condens. Matter Mater. Phys.* **2011**, *83*, 195131.
(105) Henkelman, G.; Uberuaga, B. P.; Jónsson, H. A climbing image nudged elastic band method for finding saddle points and minimum energy paths. *J. Chem. Phys.* **2000**, *113*, 9901−9904.
(106) Henkelman, G.; Jónsson, H. A dimer method for finding saddle points on high dimensional potential surfaces using only first derivatives. *J. Chem. Phys.* **1999**, *111*, 7010−7022.
(107) Timothy, J. B.; Stephen, D.; Thomas, R. F.; Shelley, L. K.; John, T. Access: Advancing innovation: NSF's advanced cyberinfrastructure coordination ecosystem: Services & support. *Practice and Experience in Advanced Research Computing*; Association for Computing Machinery: Portland, OR, USA, 2023; pp 173−176.

https://doi.org/10.1021/jacs.3c06888
J. Am. Chem. Soc. 2023, 145, 26038−26051